Global stability of swept flow around a parabolic body: Connecting attachment-line and crossflow modes

C.J. Mack, Peter J. Schmid, J.L. Sesterhenn

J. Fluid Mech. (2008), *vol.* 611, *pp.* 205–214.
doi:10.1017/S0022112008002851 Printed in the United Kingdom

Global stability of swept flow around a parabolic body: connecting attachment-line and crossflow modes

CHRISTOPH J. MACK[1], PETER J. SCHMID[2] AND JÖRN L. SESTERHENN[1]

[1]Department of Numerical Mathematics, Universität der Bundeswehr (UniBw), D-85577 Munich, Germany

[2]Laboratoire d'Hydrodynamique (LadHyX), CNRS-École Polytechnique, F-91128 Palaiseau, France

(Received 20 February 2008 and in revised form 24 June 2008)

The global linear stability of a three-dimensional compressible flow around a yawed parabolic body of infinite span is investigated using an iterative eigenvalue method in conjunction with direct numerical simulations. The computed global spectrum shows an unstable branch consisting of three-dimensional boundary layer modes whose amplitude distributions exhibit typical characteristics of both attachment-line and crossflow modes. In particular, global eigenfunctions with smaller phase velocities display a more pronounced structure near the stagnation line, reminiscent of attachment-line modes while still featuring strong crossflow vortices further downstream. This analysis establishes a link between the two prevailing instability mechanisms on a swept parabolic body which, so far, have only been studied separately and locally. A parameter study shows maximum modal growth for a spanwise wavenumber of $\beta = 0.213$, suggesting a preferred disturbance length scale in the sweep direction.

1. Introduction

The aerodynamic design of high-performance aircraft crucially depends on a sound understanding of the compressible flow around swept wings. The details of the transition process from laminar to turbulent fluid motion play a dominant role in the description of this flow. Two instability mechanisms have been suggested to trigger transition: the amplification of perturbations in the swept attachment-line boundary layer and of crossflow vortices in the three-dimensional boundary layer further downstream. These two instability mechanisms have been studied separately, despite a general acknowledgment that they coexist under realistic conditions. The subdivision of the flow configuration and the resulting separate treatment of these two instability mechanisms has been a necessary simplification of the complex flow problem in order to treat it with classical tools of hydrodynamic stability theory. Owing to the recent progress in computational resources and in global stability analysis, however, we are now able to address a more realistic configuration that covers simultaneously attachment-line and crossflow vortex instabilities. Note, however, that the notion of two independent instability mechanisms has more of an historical than a physical origin.

First evidence for the interaction of instabilities near the leading edge with the crossflow vortices further downstream came from the experiments of Gray (1952). He

found that by increasing the sweep angle, the location where the onset of transition was observed moved toward the attachment line. In following decades a great number of experimental efforts addressed instability issues for both the attachment-line boundary layer and, even more so, the three-dimensional boundary layer (see Bippes 1999; Saric, Reed & White 2003 for a recent review). Among this body of literature, Poll (1979) was the first to establish a distinction between crossflow-induced transition and transition initiated by leading-edge instabilities. His measurements on an immersed swept cylinder provided motivation for theoretical investigations.

A simplified model of the attachment-line boundary layer was studied by Hall, Malik & Poll (1984) who demonstrated that this flow becomes linearly unstable to wave-like disturbances propagating along the attachment line. This model was based on swept Hiemenz flow, which represents a similarity solution of the incompressible three-dimensional Navier–Stokes equations for swept attachment-line flow, and the Görtler–Hämmerlin assumption, which takes the same linear x-dependence for the perturbation and the base flow. Subsequently, Lin & Malik (1996) discarded the restrictive Görtler–Hämmerlin assumption and uncovered additional linearly unstable modes. They extended their analysis to compressible flows (Lin & Malik 1995) and also assessed the influence of the leading-edge curvature on flow stability (Lin & Malik 1997). A recent overview of attachment-line instabilities is given in Le Duc, Sesterhenn & Friedrich (2006).

Further downstream, the presence of sweep and curvature significantly modifies the flow. An imbalance between centrifugal forces and the streamwise pressure gradient induces curved streamlines throughout the boundary layer, and the resulting crossflow velocity gives rise to stationary or travelling crossflow vortices (Reed & Saric 1989). In contrast to the attachment-line instability, the crossflow instability is of inviscid type caused by an inflection point in the three-dimensional base velocity profile. Numerous theoretical and numerical efforts have studied the stability of compressible crossflow vortices for planar geometries, based on the parabolized stability equations (e.g. Herbert 1997) or direct numerical simulations (e.g. Joslin 1995); for an overview of the relevant literature see Saric *et al.* (2003) and the references therein.

Despite many studies of each instability, little is known to date about a connection between the two. Starting from incompressible swept Hiemenz flow, Spalart (1988) obtained solutions off the attachment line that are strongly reminiscent of crossflow vortices and thus provide a first indication of a link between them. Bertolotti (1999), using the parabolized stability equations, furnishes strong evidence for a connection between attachment-line instabilities and crossflow vortices. By continuing an attachment-line mode significantly far downstream, he finds a close match – both in terms of growth rate and modal shape – with the least-stable crossflow mode. The structure of the entire mode connecting the attachment-line and the crossflow neutral point, however, was not examined.

This lack of a connecting mode as well as the findings above strongly suggest a global treatment of the stability problem without limiting assumptions regarding the geometrical domain of interest. Such an investigation allows the simultaneous treatment of the attachment-line instability and crossflow vortices. Modern techniques such as iterative eigenvalue methods (Edwards *et al.* 1994) in conjunction with direct numerical simulations based on higher-order spatial discretization schemes provide the necessary tools to address the global stability problem. In this article, we present results from a global stability analysis of compressible flow around a swept parabolic body which demonstrate a connection between the two prevailing local instability mechanisms.

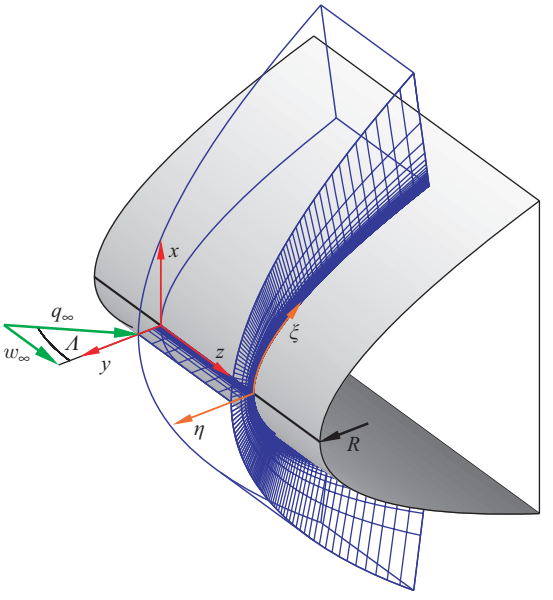

FIGURE 1. Sketch of the three-dimensional flow configuration showing the relevant flow parameters, the coordinate systems and the grid-point distribution.

2. Flow configuration, governing parameters and numerical method

The flow configuration, as displayed in figure 1, consists of a parabolic body (in grey) about which a three-dimensional body-fitted grid (in blue) is mapped. The local Cartesian coordinate system (in red) is given by the x-direction, the y-direction and the spanwise z-direction pointing along the attachment line (in black), and the local parabolic coordinate system (in orange) consists of the chordwise ξ-direction and the normal η-direction pointing along grid lines in the downstream direction and normal to the wall, respectively. The leading-edge radius of the parabolic body is denoted by R. The incoming flow impinges on the body with a velocity q_∞ and a sweep angle Λ yielding a sweep velocity w_∞ and a wall-normal velocity v_∞. The subscript ∞ refers to the flow state downstream of a detached bow shock which acts as the inflow boundary.

We define a viscous length scale δ, a sweep Reynolds number Re_s and a sweep Mach number Ma_s as

$$\delta = \left(\frac{\nu_r}{S}\right)^{1/2}, \qquad Re_s = \frac{w_\infty \delta}{\nu_r}, \qquad Ma_s = \frac{w_\infty}{c_\infty}, \tag{2.1}$$

respectively, where ν_r denotes the kinematic viscosity evaluated at recovery temperature, S is the strain rate at the wall, at the attachment line ($x = 0$), and c_∞ is the speed of sound. Alternatively, the Reynolds number Re_s can be reformulated to display an explicit dependence on the leading-edge radius R and the sweep angle Λ. We obtain (in accordance with Lin & Malik 1997, up to a scaling factor)

$$Re_s = \left(\frac{v_\infty R}{2\nu_r}\right)^{1/2} \tan\Lambda. \tag{2.2}$$

We consider the motion of a compressible fluid modelled as a perfect gas with constant specific heat ratio $\gamma = 1.4$ and constant Prandtl number $Pr = 0.71$. The compressible Navier–Stokes equations, the equation of state, Fourier's law for the

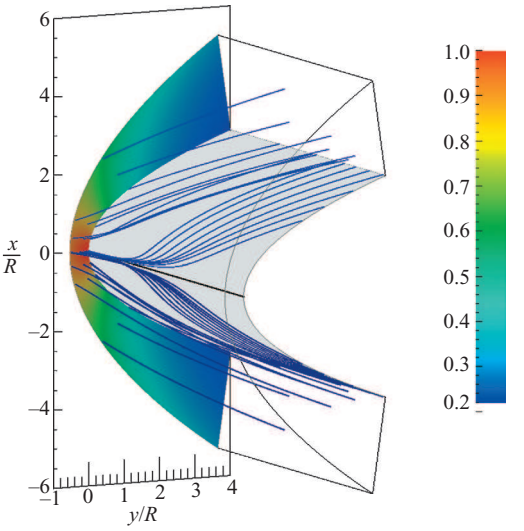

FIGURE 2. Streamlines (in blue) and pressure field of the computed steady base flow for $Re_s = 800$ and $Ma_s = 1.25$. The pressure has been non-dimensionalized by the stagnation pressure, and a leading-edge radius of $R = 0.1 = 508\delta$ has been used. The resolution is 128×255 points in the normal η-direction and the chordwise ξ-direction, respectively.

thermal conductivity and Sutherland's law (at ambient conditions) for the viscosity fully describe the flow. The equations are formulated based on pressure p, Cartesian velocities (u, v, w) and entropy s and are solved on a time-dependent, curvilinear and non-uniformly distributed grid, with a clustering of the grid points towards the wall as well as in the leading-edge region, as shown in figure 1. The governing equations are discretized using fifth- and fourth-order compact difference schemes for the inviscid and viscous terms, respectively, and a resolution of 128×255 points was used to resolve the characteristic length scales of the eigenmodes with more than six points in the normal η-direction and approximately four points in the chordwise ξ-direction. The temporal discretization is accomplished by a fourth-order Runge–Kutta scheme (see Sesterhenn 2001; Le Duc *et al.* 2006, for details).

In the wall-normal direction, the computational domain is limited by a detached unsteady bow shock which is incorporated through a shock-fitting mechanism (Fabre, Jacquin & Sesterhenn 2001) and provides the inflow conditions via the Rankine–Hugoniot relations (see Oswatitsch 1956). Along the surface of the body no-slip boundary conditions and adiabatic wall conditions are applied. At the chordwise edges of the computational domain, non-reflecting outflow boundary conditions are imposed and, under the assumption of infinite span, periodic boundary conditions are used in the z-direction.

3. Global stability analysis

The two-dimensional base flow $\phi_0(x, y)$ is stable to two-dimensional perturbations, which allows a simple time-integration toward a steady state and avoids more sophisticated methods such as Newton iteration, arclength continuation or selective filter techniques to compute the steady state. The obtained base flow forms the foundation for the subsequent global stability analysis and is displayed, in terms of streamlines and pressure field, in figure 2. The complexity of the base flow requires a

global stability approach since the x- and y-coordinate directions can no longer be separated. For this reason, a three-dimensional small-amplitude perturbation $\phi'(x, y, z, t)$ is superimposed on the base flow, and the travelling-wave form

$$\phi'(x, y, z, t) = \widetilde{\phi}(x, y)\mathrm{e}^{\mathrm{i}(\beta z - \omega t)} \tag{3.1}$$

is assumed. In this expression, $\widetilde{\phi}(x, y)$ denotes the complex amplitude and β the real spanwise wavenumber of the perturbation. The temporal long-term evolution of this disturbance is characterized by ω whose real part describes the frequency ω_r with the imaginary part as the corresponding growth rate ω_i.

Under these assumptions, the global stability problem can formally be written as

$$\omega\ \widetilde{\phi} = \mathscr{J}(\phi_0)\ \widetilde{\phi}, \tag{3.2}$$

where $\mathscr{J}(\phi_0)$ represents the linear stability operator (the Jacobian), i.e. the Navier–Stokes equations linearized about the base state ϕ_0. The direct solution of this eigenvalue problem is prohibitively expensive, and iterative solution techniques have to be employed to extract pertinent stability information. To this end, an m-dimensional Krylov subspace sequence

$$\mathscr{K}_m\{\phi, \mathscr{J}(\phi_0)\} = \mathrm{span}\{\phi,\ \mathscr{J}(\phi_0)\phi,\ \mathscr{J}(\phi_0)^2\phi, \ldots, \mathscr{J}(\phi_0)^{m-1}\phi\}, \tag{3.3}$$

consisting of repeated applications of the Jacobian matrix to a given initial flow field ϕ is used in connection with the Arnoldi method (see Edwards *et al.* 1994 for applications of iterative techniques in fluid mechanics) to project the full stability problem onto a lower-dimensional system. The resulting lower-dimensional Hessenberg matrix together with an orthonormalized basis of the Krylov subspace $\mathscr{K}_m$ can then be used to approximate the spectrum of the linearized compressible Navier–Stokes equations.

The form of the Krylov sequence (3.3) indicates that the Jacobian matrix does not need to be formed explicitly; rather, only matrix–vector products are necessary to build the reduced system. Such products are readily obtained from direct numerical simulations via

$$\mathscr{J}(\phi_0)\phi \approx \frac{\mathscr{F}(\phi_0 + \epsilon\phi) - \mathscr{F}(\phi_0)}{\epsilon}, \tag{3.4}$$

where ϵ is a small parameter, chosen as $||\epsilon\phi||/||\phi_0|| = 10^{-8}$, and $\mathscr{F}$ represents the nonlinear Navier–Stokes equations. The independence of the results with respect to the choice of the parameter ϵ has been corroborated over a range of many decades of the value of ϵ. This approximation allows a Jacobian-free framework where the direct numerical simulation provides the input for the iterative stability solver.

4. Results

The above iterative scheme is applied to simulations of the compressible flow about the parabolic body depicted in figure 1. As the Krylov subspace is augmented by subsequent calls to the direct simulation code, the Arnoldi method provides an approximate spectrum that consequently increases in complexity but also in accuracy.

4.1. *Spectrum and global modes*

The global spectrum reflects the richness of physical processes present in the flow configuration under investigation. It consists of acoustic branches that describe the presence of sound waves, of wavepacket modes that capture the dynamics of perturbations at the edge of the boundary layer, of continuous modes that represent disturbances in the free stream, of modes that account for the interaction of the bow

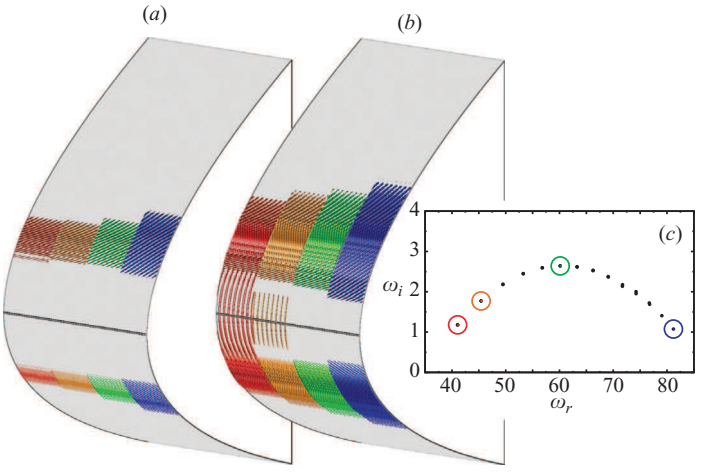

FIGURE 3. Global stability results of compressible swept flow around a parabolic body ($Re_s = 800$, $Ma_s = 1.25$, $\beta = 0.314 = 2\pi/L_z$): (c) most unstable branch of the temporal spectrum and (a, b) four associated global modes displaying the velocity distribution $v(x, y, z) = \mathrm{Re}\{\widetilde{v}(x, y)(\sin\beta z + \mathrm{i}\cos\beta z)\}$ of four eigenvalues depicted by circles in (c). The normalized eigenfunctions are plotted using iso-surfaces with a value of 10^{-2} v_{max} (a) and 5×10^{-5} v_{max} (b), and eight wavelengths, stretched by a factor of two, in the spanwise direction are used to visualize each mode (attachment line in black). See text for colour coding.

shock with the body's leading-edge region, and of shear modes that express the flow characteristics in the boundary layer. These latter modes are the most unstable ones for the present flow configuration and are the focus of this study.

Concentrating on boundary layer modes, the global stability analysis reveals that, for our flow parameters ($Re_s = 800$, $Ma_s = 1.25$, $\beta = 0.314 = 2\pi/L_z$, with L_z as the fundamental length scale, non-dimensionalized by δ, in the spanwise z-direction), a three-dimensionally unstable discrete branch is present whose disturbance frequencies ω_r range from 41.1 to 81.2 (see figure 3c). The maximum growth rate $\omega_i = 2.64$ is achieved for a frequency $\omega_r = 60.1$. Though barely visible in the figure, the eigenvalues appear double – a consequence of the symmetry properties of the flow. The associated global eigenmodes divide into symmetric and antisymmetric functions with respect to the attachment line.

Figure 3(a, b) displays four global eigenmodes from this branch, visualized by iso-surfaces (10^{-2} v_{max} (a) and 5×10^{-5} v_{max} (b)) of the normalized velocity $v(x, y, z) = \mathrm{Re}\{\widetilde{v}(x, y)(\sin\beta z + \mathrm{i}\cos\beta z)\}$. They belong to the slowest moving mode (in red), the second slowest moving mode (in orange), the most unstable mode (in green) and the fastest moving mode (in blue). The amplitude distribution of the slowest moving global mode clearly demonstrates a link between the attachment-line and the crossflow dynamics (figure 3b). It convincingly shows that the global modes of the branch depicted in figure 3(c) have typical attachment-line properties while still connecting to the familiar crossflow pattern further downstream from the stagnation line.

For faster moving global eigenfunctions (modes with a higher phase velocity ω_r) the crossflow component is more pronounced and the dominant part of the global mode lies further downstream from the leading edge. At the same time, owing to the increasing base velocity in the boundary layer, global modes with higher phase velocities prevail downstream from the attachment line.

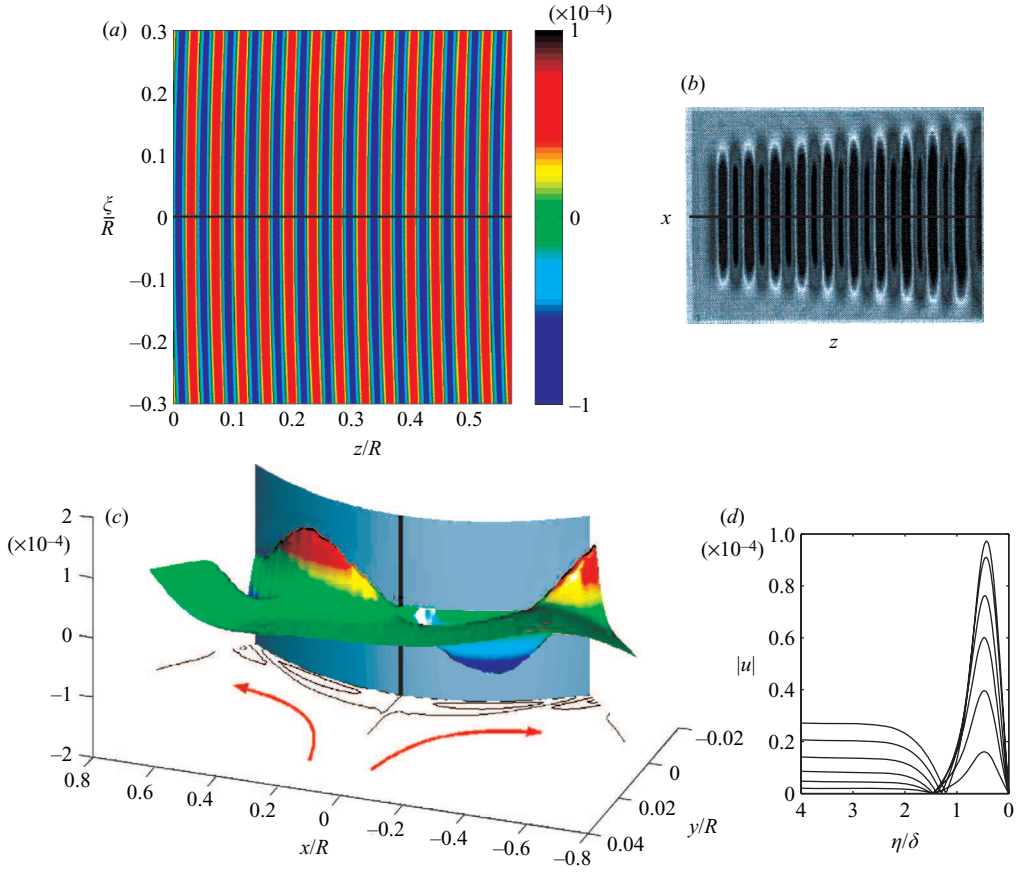

FIGURE 4. Spatial shape of the slowest moving global mode: (*a*) top view of the velocity component $v(\xi, \eta, z)$ near the attachment line in the chordwise ξ-direction at half the boundary-layer thickness ($R = 0.1 = 508\delta$); (*b*) top view of three-dimensional travelling mode $v(x, y, z)$ in an incompressible attachment-line boundary layer as presented by Joslin (1995) for $Re = 570$ and $\omega = 0.1249$ (attachment line in black, relabelled coordinate system). (*c*) Shape of the velocity component $u(x, y, z)$ in the (x,y)-plane near the attachment line and (*d*) equispaced cross-cut profiles of $u(\xi, \eta, z)$ at six selected positions in the positive ξ-direction.

Near the attachment line the global modes display the well-known and well-studied two-dimensional structure consisting of chordwise vortices with a specific spanwise scale. This structure is more pronounced for slower moving modes (see figure 3*c*). As an example, the spatial shape of the velocity component $v(x, y, z)$ of the slowest moving global mode (see figure 3*b* in red) is presented in figure 4(*a*). This mode travels along the attachment line without significant three-dimensional features. It is reminiscent of results from stability computations by Joslin (1995) (see figure 4*b*) who computed the spatial evolution of three-dimensional disturbances in an incompressible attachment-line boundary layer by direct numerical simulations for the Reynolds number $Re = 570$ and the disturbance frequency $\omega = 0.1249$. The same types of structure has been determined by Guégan, Schmid & Huerre (2006) in studies of optimal temporal disturbances in swept Hiemenz flow. However, the similarity between these two incompressible results and our compressible result is only of a qualitative nature. Further evidence linking the local behaviour of the global mode

near the stagnation line to a typical local attachment-line mode is given in figure 4(*c*) where the characteristic linear dependence in the chordwise direction of the velocity component $u(x, y, z)$ is visible over a significant range along the attachment line before it saturates to connect to the crossflow behaviour further downstream. In addition, figure 4(*d*) displays equispaced cross-cut profiles of $u(\xi, \eta, z)$ at six selected positions in the positive ξ-direction, which closely resemble the corresponding eigenfunction shapes from a solution of a modal stability problem for swept Hiemenz flow.

Further downstream in the chordwise direction, the initially two-dimensional structure of the global mode near the attachment line (see figure 4*a*) gradually merges into a three-dimensional one (see figure 5*a*) until the vortical structures nearly align with the external streamlines, resulting in co-rotating vortices (see figure 5*b*), a feature that is specific to crossflow vortices as described by Reed & Saric (1989).

As detailed above, the compressible flow around a swept parabolic body is governed by a large number of parameters describing various flow quantities, fluid properties and geometric characteristics. Even though the above observations are expected to hold for a wide range of parameters, we chose to present a parametric study of the global stability properties with respect to the spanwise wavenumber β. The computed temporal global spectrum consisting of growth rate ω_i and frequency ω_r is shown in figure 6(*a*) for selected spanwise wavenumbers ranging from 0.090 to 0.314. The typical parabolic shapes of the unstable boundary layer branch are clearly visible where smaller phase velocities are observed for smaller spanwise wavenumbers. The growth rates ω_i appear to grow steadily up to a specific spanwise wavenumber before decaying again. The spanwise wavenumber at which a maximum modal growth is observed has been determined to be $\beta = 0.213$ (see figure 6*b*), thereby pointing toward a preferred disturbance length scale (or scale selection mechanism) in the spanwise direction.

Parenthetically, one can see more clearly in figure 6(*a*) that the boundary layer branch consists of double eigenvalues. For some parameter combinations, the eigenvalue pairs at the edge of the parabola separate slightly, which is a typical aliasing phenomenon caused by a marginal numerical resolution of the corresponding global eigenfunctions.

5. Discussion and conclusions

A global stability analysis of compressible flow around a yawed parabolic body has numerically established a link between attachment-line modes and crossflow modes. Though for the parameters studied in this article the crossflow vortices represent the largest amplitude component of the global boundary layer mode, eigenfunctions from the slower part of the unstable branch displayed the characteristic two-dimensionality and linear chordwise dependence (in the chordwise velocity) of a typical attachment-line mode. We thus conclude that the global spectrum of flow around a swept parabolic body contains combination modes that display typical features of both local crossflow vortices and local attachment-line instabilities. In this sense, the study of attachment-line or crossflow instabilities in a separate and local setting is simply the respective local approximation of one of these global combination modes. Consequently, this investigation adds to the previous study by Bertolotti (1999) in establishing a link between attachment-line and crossflow modes. In addition, it provides numerical evidence for the experimental observations of Gray (1952). A most preferred spanwise scale has been found; since it is given by global modes with a dominant crossflow component, it is expected that the crossflow vortices will imprint their favoured spanwise length scale onto the entire flow.

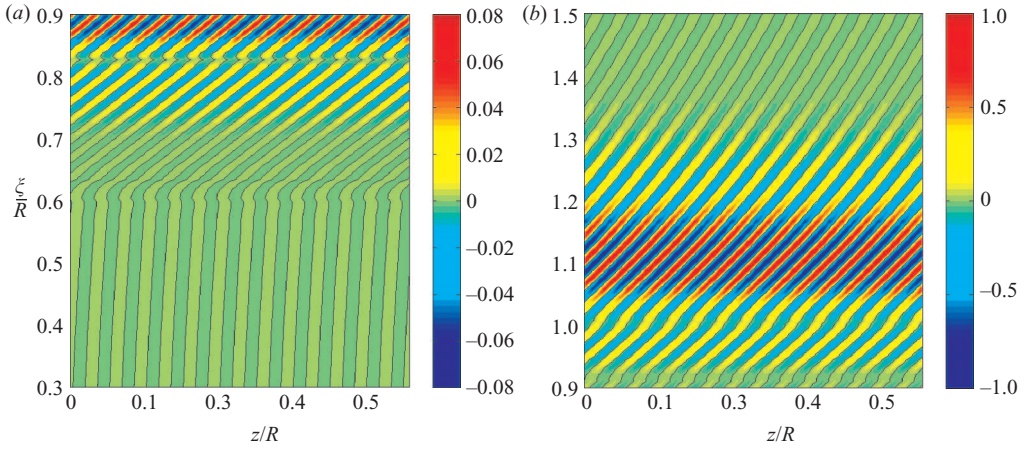

FIGURE 5. Spatial shape of the velocity component $v(\xi, \eta, z)$ of the slowest moving global mode in a body-fitted cut at half the boundary-layer thickness: (*a*) structure in the connection region and (*b*) structure further downstream in the positive ξ-direction (iso-contour lines of zero amplitude in black).

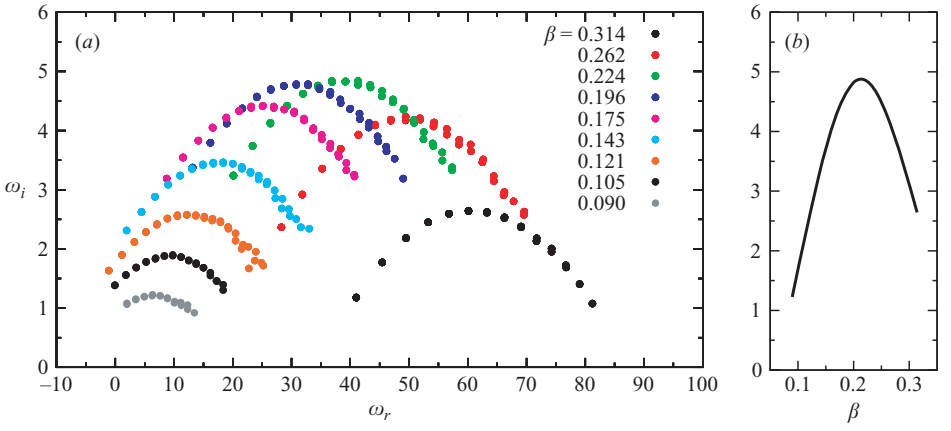

FIGURE 6. (*a*) Temporal spectra from global stability calculations for selected spanwise disturbance wavenumbers β; (*b*) temporal growth rate ω_i as a function of β.

Besides the stability characteristics of the attachment-line and crossflow modes presented in this article, the receptivity of the global modes to external excitations or wall roughness distributions is important for industrial applications. An analysis of this type (which is beyond the scope of this investigation) will reveal the mechanisms that excite dominant structures in the flow about a blunt body, be it by direct excitation of the crossflow modes or by forcing of structures near the attachment line that, in turn, initiate the growth of crossflow vortices via the connection demonstrated in this study.

On a more methodological point, the combination of iterative eigenvalue algorithms and direct numerical simulations has proved to be an effective tool in addressing complex stability problems in their entirety instead of via piecewise local approximations. Many more flow configurations of academic or technological interest await analysis in the manner described in this article.

Financial support from the Deutsche Forschungsgemeinschaft (DFG), the Studienstiftung des Deutschen Volkes and the Alexander-von-Humboldt Foundation is gratefully acknowledged. Patrick Huerre is warmly thanked for his insightful comments on the manuscript.

REFERENCES

Bertolotti, F. P. 1999 On the connection between cross-flow vortices and attachment-line instabilities. In *IUTAM Symp. on Laminar-Turbulent Transition*, pp. 625–630. Sedona, USA.

Bippes, H. 1999 Basic experiments on transition in three-dimensional boundary layers dominated by crossflow instability. *Prog. Aero. Sci.* **35**, 363–412.

Edwards, W. S., Tuckerman, L. S., Friesner, R. A. & Sorensen, D. C. 1994 Krylov methods for the incompressible Navier–Stokes equations. *J. Comput. Phys.* **110**, 82–102.

Fabre, D., Jacquin, L. & Sesterhenn, J. 2001 Linear interaction of a cylindrical entropy spot with a shock. *Phys. Fluids* **13** (8), 2403–2422.

Gray, W. E. 1952 The effect of wing sweep on laminar flow. *Tech. Rep.* RAE TM Aero 255. British Royal Aircraft Establishment.

Guégan, A., Schmid, P. J. & Huerre, P. 2006 Optimal energy growth and optimal control in swept Hiemenz flow. *J. Fluid Mech.* **566**, 11–45.

Hall, P., Malik, M. & Poll, D. I. A. 1984 On the stability of an infinite swept attachment-line boundary layer. *Proc. R. Soc. Lond.* A **395**, 229–245.

Herbert, T. 1997 Parabolized stability equations. *Annu. Rev. Fluid Mech.* **29**, 245–283.

Joslin, R. D. 1995 Direct simulation of evolution and control of three-dimensional instabilities in attachment-line boundary layers. *J. Fluid Mech.* **291**, 369–392.

Le Duc, A., Sesterhenn, J. & Friedrich, R. 2006 Instabilities in compressible attachment-line boundary layers. *Phys. Fluids* **18**, 044102.

Lin, R. S. & Malik, M. R. 1995 Stability and transition in compressible attachment-line boundary-layer flow. *Tech. Rep.* 952041. SAE.

Lin, R. S. & Malik, M. R. 1996 On the stability of attachment-line boundary layers. Part 1. The incompressible swept Hiemenz flow. *J. Fluid Mech.* **311**, 239–255.

Lin, R. S. & Malik, M. R. 1997 On the stability of attachment-line boundary layers. Part 2. The effect of leading edge curvature. *J. Fluid Mech.* **333**, 125–137.

Oswatitsch, K. 1956 *Gas Dynamics*. Academic.

Poll, D. I. A. 1979 Transition in the infinite swept attachment-line boundary layer. *Aero. Q.* **30**, 607–628.

Reed, H. L. & Saric, W. S. 1989 Stability of three-dimensional boundary layers. *Annu. Rev. Fluid Mech.* **21**, 235–284.

Saric, W. S., Reed, H. L. & White, E. B. 2003 Stability and transition of three-dimensional boundary layers. *Annu. Rev. Fluid Mech.* **35**, 413–440.

Sesterhenn, J. 2001 A characteristic-type formulation of the Navier–Stokes equations for high-order upwind schemes. *Comput. Fluids* **30**, 37–67.

Spalart, P. R. 1988 Direct numerical study of leading-edge contamination. In *AGARD-CP-438*, pp. 5/1–5/13.